

In vivo MRI measurements of tumor growth induced by dichloroacetate: implications for mode of action

J.H. Miller, K. Minard, R.A. Wind, G.A. Orner, L.B. Sasser, R.J. Bull *

Pacific Northwest National Laboratory, Molecular Biosciences, PO Box 999-P7-56, Richland, WA 99352, USA

Received 14 September 1999; accepted 8 December 1999

Abstract

Dichloroacetate (DCA) is an important by-product of the chlorination of drinking water that produces liver cancer in rodents. Assessment of the risk that results from concentrations that occur in drinking water will be dependent upon the mode of action held responsible for these tumors. A study by Stauber and Bull [Stauber, A.J. and Bull, R.J. (1997) Differences in phenotype and cell replicative behavior of hepatic tumors induced by dichloroacetate (DCA) and trichloroacetate (TCA). *Toxicol. Appl. Pharmacol.* 144, 235–246] in mice treated with DCA demonstrated a lesion distribution that was skewed towards many small, altered foci of cells that are assumed to be precursor lesions [EPA, (1996). U.S. Environmental Protection Agency: Proposed Guidelines for carcinogen risk assessment; notice. *Fed. Reg.* 61, pp. 17 960–10 811]. The present study was designed to determine the extent to which the tumorigenic effects of DCA could be explained by its effect on tumor growth rates (i.e. tumor promoting activity). In vivo magnetic resonance imaging (MRI) allowed accurate determination of growth rates of individual lesions in mice that had been treated with DCA in drinking water at 2 g/l. Out of thirty treated mice, ten were found to have hepatic tumors detectable by MRI at 48 weeks of treatment. These tumor-bearing animals were assigned to two groups matched on the size of lesions observed by in vivo MRI. Treatment with DCA continued in one group of five mice and was stopped in the other. For both groups, tumor growth rates were determined by measuring changes in size of all lesions greater than 1 mm³ in volume during a 14-day period. Removal of DCA treatment resulted in growth rates that could not be distinguished from zero across all lesion sizes represented in the sample. These data are in agreement with previous observations of DCAs effects on replication rates within tumors (Stauber and Bull, (1997)). Tumor growth rates observed in animals maintained on treatment decreased with lesion volume in a manner that is consistent with a stochastic Gompertz birth-death process proposed by Tan [Tan, W.Y. (1986) A stochastic Gompertz birth-death process. *Stat. Prob. Lett.* 4, 25–28]. Parameters of this model obtained by fitting measured growth rates were used to predict the lesion-size distribution expected after one year of DCA treatment. The shape of the predicted lesion-size distribution was similar to that observed by Stauber and Bull (Stauber and Bull, (1997)) in mice sacrificed after 40 weeks of DCA treatment. We conclude that the effects of DCA on the division and/or death rates of spontaneously initiated cells can account for the predominance of small lesions in DCA-treated animals. © 2000 Published by Elsevier Science Ireland Ltd. All rights reserved.

* Corresponding author. Tel.: +1-509-3736218; fax: +1-509-3766767.
E-mail address: dick.bull@pnl.gov (R.J. Bull)

Keywords: Dichloroacetate; Liver cancer; Mice; MRI; Tumor growth; Tumor promotion

1. Introduction

Dichloroacetate (DCA) is one of the most prominent by-products of the chlorination of drinking water. It occurs in chlorinated drinking water at median concentrations of 13 $\mu\text{g/l}$ (10th and 90th percentile concentrations are 2.1 and 31 $\mu\text{g/l}$, respectively) (Krasner et al., 1989). At high doses (≥ 0.5 g/l) DCA is efficient as an inducer of liver tumors in B6C3F1 mice (Herren-Freund et al., 1987; Bull et al., 1990; DeAngelo et al., 1991; Daniel et al., 1992; Pereira, 1996; Stauber and Bull, 1997) and in F344 rats (DeAngelo et al., 1996). Recent studies have identified mutagenic effects of DCA in *Salmonella* (Giller et al., 1997) and in the mouse lymphoma assay (Harrington-Brock et al., 1998) at very high concentrations of DCA (≥ 1 mM). Previous studies in *Salmonella* (Fox et al., 1996), which focused on lower concentrations and used different methods, were largely negative. Tumors and altered hepatic foci (AHF) induced by DCA have a size distribution that is skewed towards smaller lesions than found with trichloroacetate (TCA), a peroxisome proliferator (Stauber and Bull, 1997). A distribution consisting largely of small lesions is frequently interpreted as an indication that a chemical possesses tumor-initiating activity (Moolgavkar et al., 1990).

There is considerable evidence that DCA acts as a tumor promoter. Pereira and Phelps (1996) demonstrated that DCA acts as a promoter of liver tumors in mice. Bull et al. (1990) found that suspension of DCA treatment at 36 weeks yielded a tumor incidence at 52 weeks that would have been predicted from the total dose administered. However, those tumors in animals whose treatment was suspended were all benign while 25% of the tumors in mice on continuous treatment were found to be carcinomas. Studies of Pereira (1996) support the contention that DCA induces a benign phenotype that does not progress if treatment is suspended early. On the other hand, DeAngelo et al. (1996) found that relatively short treatments with DCA (10–20 weeks) at high doses (3.5 g/l) still produced a high incidence of hepato-

cellular tumors over the lifetime of the animal. Stauber and Bull (1997) reported that DCA appeared to induce a relatively benign phenotype based on replication rates following suspension of treatment for two weeks. The replication rates remained at twice the basal level in animals that were maintained on DCA treatment (2 g/l). This stimulation of cell replication occurred only with treatment concentrations ≥ 2 g/l (Stauber and Bull, 1997) despite the fact that 0.5 g/l produces $> 80\%$ tumor incidence in lifetime experiments (Daniel et al., 1992). The major difference with higher doses is an earlier appearance of multiple tumors (Bull et al., 1990). Thus, circumstantial evidence strongly suggests that high doses of DCA greatly affect growth rates of tumors, but there have been no direct measurements.

Magnetic resonance imaging (MRI) provides a means of observing changes in the size of the same tumor over time in situ. Using this tool, we have directly tested the hypothesis that high doses of DCA influence the growth rates of hepatic tumors. By making measurements of how growth rate varies with lesion size under the influence of DCA-treatment, the size distribution of the lesions can be predicted. This allowed us to pursue a second objective of determining if the size distribution of lesions that were observed in prior studies (Stauber and Bull, 1997) could be explained by assuming a spontaneous mutation rate exacerbated by suppression of apoptosis and increases in tumor cell replication rate by DCA.

2. Materials and methods

2.1. Chemicals

Analytical grade dichloroacetic acid (DCA) was purchased from Fluka Chemical Corporation (Ronkonkoma, NY). Analysis by a gas chromatograph equipped with an electron capture detector indicated that the DCA was $> 99\%$ pure. Drinking water containing DCA was prepared for the mice using double distilled water and neutral-

ized with sodium hydroxide to a pH between 6.8–7.2. The final concentration was 2.0 g/l, calculated as the free acid. Prior work has demonstrated that DCA is stable in water for at least 1 month (Bull et al., 1990).

2.2. *Animals and DCA exposure protocol*

Thirty, six-week-old male B6C3F1 mice were purchased from Charles River Laboratories (Raleigh, NC), allowed to acclimate for 1 week, and subsequently placed on DCA treatment. All animal care, use, and experimental protocols were approved by the Institutional Animal Care and Use Committee (IACIC) at Pacific Northwest National Laboratory. Mice were treated with 2.0 g/l DCA in their drinking water for 48 weeks. This treatment period was sufficiently long to ensure the induction of small liver tumors (Bull et al., 1990; Stauber and Bull, 1997). It also coincided with the treatment duration used in previous work where MR imaging was originally shown to be highly sensitive for detecting DCA-induced lesions in vivo (Minard et al., 1997). At 48 weeks of DCA treatment, MR imaging found tumors in 10 mice. A total of 13 tumors were identified in these 10 mice. Following the first MR imaging session, mice with lesions of comparable size were randomly assigned to two treatment groups of five animals apiece. One group was maintained on DCA treatment and the other received double-distilled water (pH 6.8–7.2) for the remainder of the study. Between two and three weeks after the first imaging session all animals were imaged again and, shortly thereafter, sacrificed so livers could be resected for visual inspection.

2.3. *In vivo MRI*

Prior to MR imaging, each mouse was anesthetized using a mixture of ketamine hydrochloride (120 mg/kg) and xylazine (7.2 mg/kg) administered intraperitoneally. Magnetic resonance images were acquired using a UNITY plus imaging spectrometer (Varian, Palo Alto, CA) and a commercial imaging probe (Doty Scientific, Columbia, SC). During MR imaging exams, the probe was mounted inside an 11.7 Tesla, 89-mil-

limeter-diameter vertical bore magnet (Oxford Instruments, Oxford, UK). Lesion visualization was facilitated using a multi-slice, T₂-weighted spin-echo sequence run with a 2 s recycle delay and a 17 ms echo time. All images were acquired in the transverse plane with a 3.5 × 3.5 cm² field of view. In all cases, twenty-five contiguous slices were sampled to cover the entire liver region with a slice thickness of 1 mm. Raw data for each slice consisted of 256 phase encoded spin-echoes each comprised of 256 frequency encoded data points collected with an acquisition bandwidth of 250 Hz/pixel. No signal averaging was used and a compact respiratory triggering device was exploited to reduce abdominal motion artifacts (Minard et al., 1998). Under these circumstances, image acquisition typically only required ≈ 8.5 min. This short time for data acquisition greatly minimizes the amount and duration of anesthesia required to immobilize the mice. Higher resolution images could have been easily obtained, but the decision was made to avoid as much stress to the animals as possible.

2.4. *Liver-lesion discrimination and volumetric analysis*

In MR images, liver tumors generally appeared hyperintense (i.e. bright) relative to normal liver tissue. However, low liver-lesion contrast sometimes prevented unambiguous definition of liver-lesion boundaries. To facilitate an unbiased volumetric analysis, a simple statistical procedure was used for discriminating between normal liver and tumor tissue in acquired MR images. In practice, this involved three steps. First, the mean liver intensity was measured in several regions-of-interest (ROIs) close to each lesion. Then, the upper limit to the 95% confidence interval for the mean liver intensity was calculated from tabulated ROI measurements. Finally, the upper limit to the mean liver intensity was used as the grayscale level threshold for acquiring image data; thereby, leaving only those pixels displayed with a 95% chance of being different from the average liver intensity.

After images were displayed and a grayscale threshold applied, tumor volumes were calculated

by manually outlining lesion boundaries in each slice. The enclosed cross-sectional area observed in each individual slice was then multiplied by the slice thickness (1.0 mm). Finally, this procedure was repeated for each slice and the results were summed to give the total volume for each tumor. Using this approach, uncertainty in measured tumor volumes arising from ambiguities in liver-lesion boundaries was quantified by outlining the minimum and maximum possible extent of each tumor. In so doing, a range of possible volumes was defined for each tumor. All image display, analysis and manipulation were performed using a commercial MR image processing package (Varian, Palo Alto, CA).

2.5. Calculation of tumor growth rates

Tumor growth was quantified assuming tumor volume increased exponentially ($e^{K\Delta T}$) during the time between successive imaging sessions (ΔT). Growth could then be described by a single rate constant (K) defined in terms of the natural logarithm and lesion volumes measured during the first (V_1) and second (V_2) imaging sessions (i.e. $K = \text{Ln}(V_2/V_1)/\Delta T$). For each lesion, the range of possible rate constants was determined by using the minimum and maximum possible lesion volumes measured from MR image data. The minimum and maximum possible rate constant for each tumor then provided a relatively crude measure of the variability involved in the measurements. Likewise midrange values provided a measure of central tendency.

3. Results

High-resolution MR images of live mice provided a basis for quantifying temporal changes in tumor volume during different DCA treatment protocols. This is illustrated in Fig. 1 where a single cross-section of a small lesion from each treatment group is displayed from MR data acquired during successive imaging sessions. In each case, the same cross-section is shown so relative changes in tumor size can be qualitatively assessed. As shown in Fig. 1, significant tumor

growth is apparent in the animal maintained on DCA treatment while little change in tumor size is evident in the animal that had DCA treatment suspended.

During MR imaging exams 80% of those lesions found at necropsy with a diameter greater than 1.0 mm were observed in acquired images. This detection sensitivity was somewhat higher than that observed in clinical MR imaging studies performed under similar conditions (Carpenter et al., 1996). DCA-induced tumors are uniform in their phenotype with respect to being both glycogen-poor and c-Jun+ (Stauber and Bull, 1997), so there was no obvious reason for the fact that the two lesions of greater than 1 mm³ were not detected by MRI.

In general, reliable measurement of growth rates requires unambiguous definition of liver-lesion boundaries. In practice, the ability to do so depends on the observed liver-lesion contrast to noise ratio (CNR). In a given image, this quantity is defined as the difference in intensity between the observed lesion and adjacent liver (contrast) all divided by the images noise variance. Unfortunately, liver-lesion contrast is notoriously low, particularly for the solid lesions of interest in the current study (Edelman et al., 1996). Moreover, since the use of exogenous contrast agents would significantly complicate long-term toxicology studies, there is no particular MR imaging method that drastically improves observed liver-lesion contrast. In fact, the T₂-weighted spin-echo sequences used in the current study are widely accepted as the gold standard for hepatic imaging (Edelman et al., 1996). Therefore, in this context, liver-lesion CNR is only improved by reducing image noise.

In the current study the average liver-lesion CNR was 3.6 ± 0.8 in acquired MR images. Compared with our earlier work, this was a factor-of-two lower. This difference was not unexpected, however, since signal averaging was previously employed as a simple means of mitigating respiratory-induced motion artifacts (Minard et al., 1997). In practice, this also reduced image noise by a factor-of-two; thereby, accounting for the relative difference between studies. Detection sensitivity in earlier work was also higher (~94%)

than reported here. Together with observed contrast-to-noise ratios, this suggests that the detection of DCA-induced lesions is primarily a function of the observed liver-lesion CNR. Specifically, as the CNR is improved, liver-lesion boundaries become less ambiguous and any particular lesion is more likely to be detected. This simple idea is consistent with histological findings. In this regard, detection of DCA-induced lesions appears to be merely a statistical manifestation of a low contrast-to-noise ratio. Consequently, conclusions drawn from the current study should not be influenced by less than perfect MR detection sensitivity.

Quantitative analysis of tumor growth kinetics using measured tumor volumes from multislice

MR image data indicated that treatment dependent differences in lesion growth were most pronounced for small lesions. This is illustrated in Fig. 2 where the calculated rate constant (K) for each lesion is plotted on a semi-log graph as a function of initial lesion volume (V_1). The graph clearly shows that small nodules and tumors (ca. 0.02–0.1 ml in volume) in mice continued on DCA treatment exhibited rapid growth while lesions of comparable size essentially stopped growing when DCA treatment was suspended.

Although efforts were made to match lesions of comparable size in different treatment groups, assignments were initially made by visually matching apparent lesion diameters observed in acquired MR images. As image-based volumetric

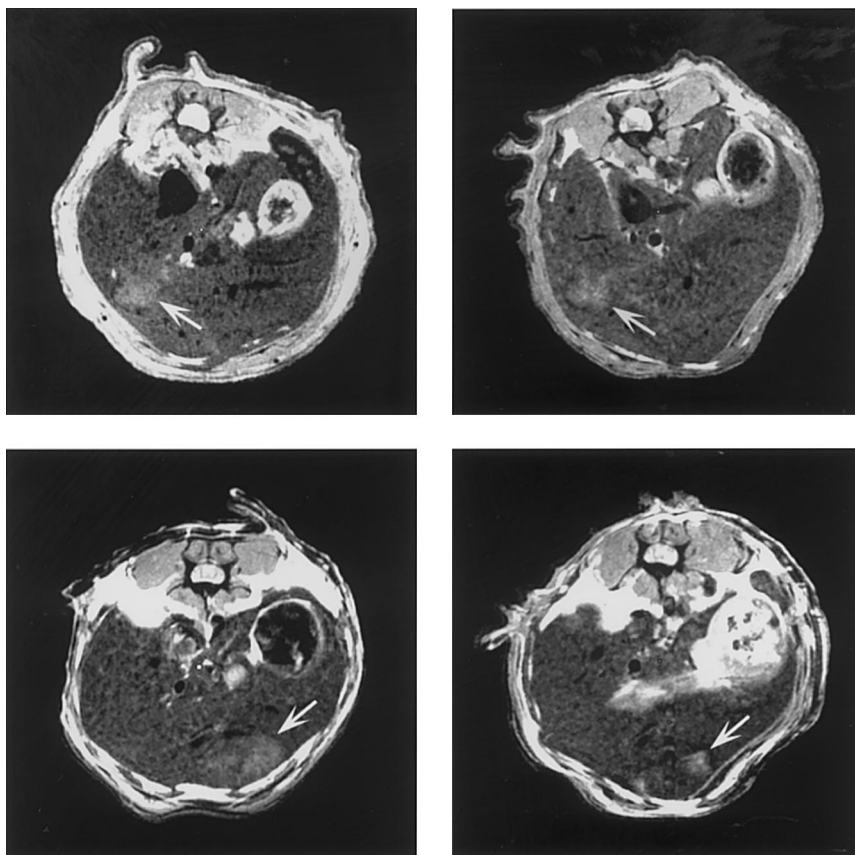


Fig. 1. MR images of two different mice—each exposed to a different DCA treatment regiment. Top row shows the same cross-section of a mouse maintained on DCA exposure (21 days between adjacent images). Bottom row shows the same cross-section of a mouse before and after suspension of chronic DCA exposure (17 days between adjacent images). In all cases, lesions are identified with white arrows.

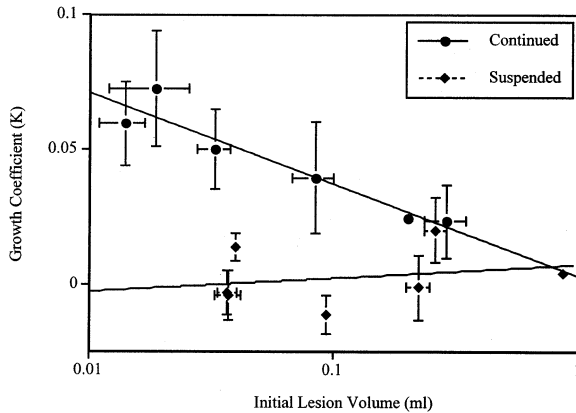


Fig. 2. Effects of suspending DCA treatment on tumor growth observed in vivo with magnetic resonance imaging—see methods section for definition of growth coefficient (K). Results of regression analysis are listed below. In both regression equations, LOG refers to the base 10 logarithm. $K = -0.034\text{LOG}(V_1) + 0.003$ {Continued}. $K = 0.005\text{LOG}(V_1) + 0.007$ {Suspended}

measurements were refined according to the procedure described in the methods section, a small bias towards smaller lesions was later found in mice continued on DCA treatment. The logarithmic scale of Fig. 2 exaggerates this difference. The initial volume for each of the three smallest lesions in each treatment group differed by no more than a factor of two and a half. Consequently, data presented in Fig. 2 provides direct evidence that DCA is responsible for virtually all of the growth of small lesions that could be measured in a 2–3 week time interval. Remarkably, the measured growth rates were consistent enough that detailed analysis of small tumors in just ten animals (5 on continued treatment; 5 on suspended treatment) was sufficient to demonstrate the phenomenon.

The size dependence of growth rates measured for lesions in mice that continued to receive DCA treatment is consistent with a model of tumor growth proposed by Tan (1986). Under the general assumption that clonal expansion is a stochastic birth-death process (see Luebeck and Moolgavkar, 1991 for details), the average size of foci initiated at time s and observed at time t is

$$N(t,s) = \exp \left\{ \int_s^t [\alpha(x) - \beta(x)] dx \right\} \quad (1)$$

where α and β are the rates of cell division and death, respectively. Tan (1986) proposed a model for the time dependence of the net growth rate $\delta(x) = \alpha(x) - \beta(x) = \lambda \exp(-x/\tau)$. Substituting this result into Eq. (1) yields

$$\begin{aligned} N(t,s) &= \exp \{ \lambda \tau [1 - \exp(-(t-s)/\tau)] \} \\ &= \exp \{ \tau [\delta_0 - \delta(t-s)] \} \end{aligned} \quad (2)$$

where $\delta_0 = \lambda$ is the initially growth rate and $\delta(t-s)$ is the growth rate after a time $t-s$ has elapsed. Solving Eq. (2) for growth rate as a function of lesion size yields the result

$$\delta = \delta_0 - \ln(N)/\tau \quad (3)$$

which predicts that growth rate will be a linear function of the natural log of lesion size with slope $-1/\tau$ and intercept δ_0 .

Linear regression analysis of the data in shown Fig. 2 allowed us to estimate a value of about 70 days for the parameter τ in Tan's model. This value is significantly longer than the period between volume measurements; hence, the approximation used to calculate growth rates from changes in lesion volume (see Section 2 for details) is justified. The initial growth rate λ can also be estimated from this regression analysis provided the number density of cells in lesions is known. This density was not measured; however, Moolgavkar et al. (1990) calculate a value of 1.4×10^8 cells per cubic centimeter based on the assumption of 12 microns for the radius of hepatocytes in enzyme-altered foci of the rat. With this cell density, we estimate a value of 18.9 for the dimensionless parameter $\lambda\tau$. With $\tau = 70$ days, this value of $\lambda\tau$ corresponds to an initial doubling time of about 4 days. From Eq. (3) one sees that $\lambda\tau$ depends on the logarithm of cell density in lesions; hence, the value derived from the data in Fig. 2 is not sensitive to the uncertainty in Moolgavkar's recommendation.

Values of the parameters λ and τ derived from the dependence of growth rates on lesion size can be used to predict the size distribution of lesions in DCA-treated mice for comparison with the results reported by Stauber and Bull (1997). The primary assumption needed to make this connection between growth rates and size distribution is

that a stochastic birth-death process governs the growth of lesions throughout the time interval between their spontaneous initiation and their observation. Implicit in this assumption is the neglect of rare events where division of an initiated cell produces a mutated daughter with different birth-death characteristics. This approximation, which is common in the analysis of foci size distributions, is consistent with the observation that DCA-treatment mainly promotes benign lesions (Pereira, 1996).

Like Chen and Farland (1991), we assume that the waiting time between entries of initiated cells into the cell cycle is an exponentially-distributed random variable with an average value of $1/\lambda$. Let d , b , and μ be the probabilities that a cell cycle terminates by death, normal division, or mutation, respectively. Then $\delta(x) = \alpha(x) - \beta(x) = \lambda[b(x) - d(x)] = \lambda \exp(-x/\tau)$ is interpreted to mean that the difference between the probabilities of division and death, which is initially unity, decays with a characteristic time τ . When this interpretation of Tan's model (1986) is combined with the fact that the probability of mutation per cell cycle is very small (i.e. $b + d \sim 1$), one arrives at the expression

$$\beta(x) = \lambda[1 - \exp(-x/\tau)]/2 \tag{4}$$

for the time-dependent death rate.

The probability of finding at least k living cells in a clone initiated at time s and observed at time t can be derived from Eq. (4) using the classical results of Kendall (1948).

$$P_k(s,t) = S(s,t)[1 - g(s,t)S(s,t)]^{k-1} \tag{5}$$

where $g(s, t)$ is the reciprocal of the average size $N(s, t)$ given by Eq. (2) and

$$S(s,t) = \left[1 + \int_s^t \beta(x)g(s,x)dx \right]^{-1} \tag{6}$$

is the probability that a clone, initiated at time s , escapes extinction until time t . Substitution of Eq. (4) into Eq. (6) gives the following analytical result for the survival probability:

$$S(s,t) = 2/\{1 + g(s,t) + \lambda\tau \exp(-\lambda\tau) [Ei(\lambda\tau) - Ei(\lambda\tau \exp(-(t-s)/\tau))]\} \tag{7}$$

Since the time of initiation was not observed in our experiments, $P_k(s, t)$ must be averaged over s using the weights $R(s)S(s, t)$, where $R(s)$ is the rate of initiation. This average can be written as

$$p_k(t) = \int_0^t S(s,t)P_k(s,t)ds / \int_0^t S(s,t)ds \tag{8}$$

if we make the additional assumption that the rate of spontaneous initiation is not time dependent.

The lesion-size distribution predicted by this model when $t = 364$ days, $\tau = 70$ days, and $\lambda\tau = 18.9$ days is shown in Fig. 3. The rapid decrease in the probability to observe larger lesions is qualitatively similar to the findings of Stauber and Bull (1997). This feature is not very sensitive to the uncertainty in the parameters λ and τ . The functional form of the survival probability in this model favors small lesions. Even though $S(s, t)$ goes to zero as time after initiation increases (see Abramowitz and Stegun, 1965 for properties of the exponential integral), it approaches this limit very slowly. A 95% probability of survival is typical at the times that contribute significantly to the integrals in Eq. (8). High survival probability in clonal expansion leads to a large number of small foci (Dewanji et al., 1989; Moolgavkar, 1989).

The size distribution shown in Fig. 3 is very similar to that predicted by the Luebeck and Moolgavkar (1991) model with the ratio of β/α fixed at a value of 0.05; however, our interpretation of Tan's time-dependent net growth rate is different from that of the Luebeck and Moolgavkar model. If β/α is constant and $\alpha - \beta$ approaches zero, then both α and β must approach zero, which means that growth saturates because cell division and death within a nonextinct clone have ceased. An alternative description of growth saturation due to a balance between cell division and death (Schulte-Hermann et al., 1993; Grasl-Kraupp et al., 1997) is more consistent with our model assumptions.

4. Discussion

In vivo MRI allows the development of individual carcinogenic lesions to be followed in time. We have used this capability to investigate the effect of treatment termination on the growth rate of lesions observed in B6C3F1 mice after 48 weeks of treatment with DCA. Among the relatively small number of lesions followed in this study, continued growth was entirely dependent of upon DCA treatment. This finding is consistent with other results (Bull et al., 1990; Pereira, 1996; Stauber and Bull, 1997) indicating that DCA mainly simulates the growth of benign liver tumors. Growth rates measured for lesions in animal continued on DCA treatment exhibited a linear decrease with the logarithm of their size at 48 weeks. This type of size distribution is consistent with a model proposed by Tan (1986) in which the average growth rate decreases exponential with time since initiation. The best fit of the model to measured rates was obtained with an initial growth rate of about 0.3 cells/day and a decay time of about 70 days.

With the growth characteristics determined by the fit of Tan's model to our data, DCA promoted lesions would be expected to reach an average volume of about 0.35 ml. Lesions with a volume significantly larger than this upper limit were observed in male B6C3F1 mice after 38 or 52 weeks of DCA treatment (Bull et al., 1990; Stauber and Bull, 1997), consequently, changes in the tumor appear necessary for growth to continue. The most general explanation is that the lesions progress as the result of additional, probably spontaneous mutations that give rise to subpopulations of cells with different birth and death rates (Farber and Sarma, 1987). Thus, it is probable that the growth rate curve obtained from our data describe an early stage in tumor development. As indicated in our prior studies (Stauber and Bull, 1997), there is a tendency for larger lesions induced by DCA to be basophilic while smaller lesions are largely eosinophilic. While this is a non-specific shift in phenotype, it may reflect differing characteristics that are required of tumors that continue to grow.

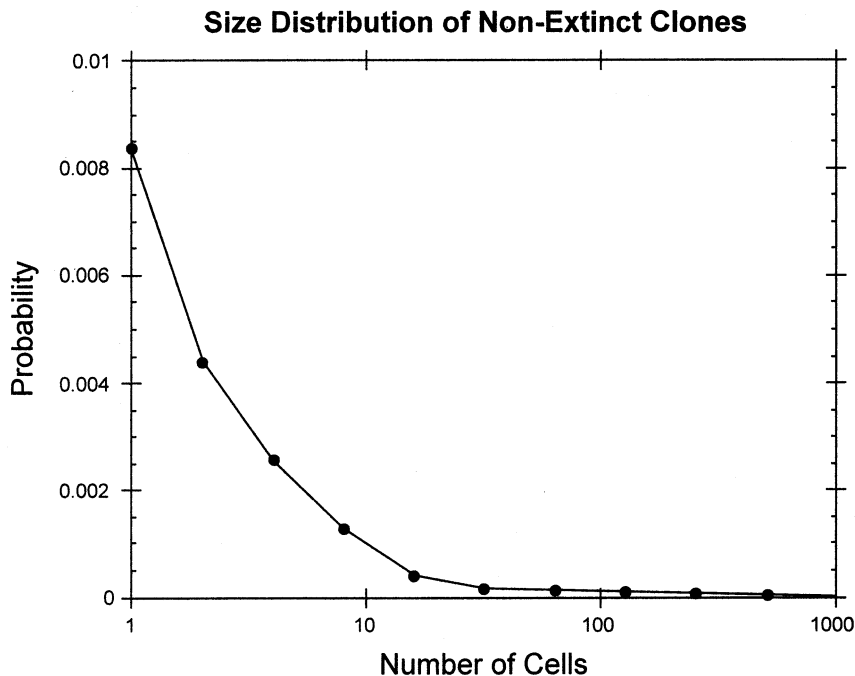


Fig. 3. The distribution of lesion sizes in animals treated by DCA for 1 year predicted from the dependence of growth rates on lesion size observed by in vivo MRI.

The mechanisms responsible for the saturation of growth cannot be deduced from the data at hand. Cell types that initially responded to the presence of DCA by entering the cell cycle may have become quiescent as their populations expanded due to insufficient access to nutrients and oxygen. Folkman et al. (1974) estimated that cells at center of a mass that had not developed vasculature would be unable to sustain proliferation when the radius exceeds about 1 mm, which corresponds to a sphere with a volume of 0.0042 ml. As the lesion grows, the center of the tumor becomes necrotic due to the lack of oxygen. Under these conditions, the lesion will continue to grow, but the fractional rate slows as the central core that is not capable of replication expands. In the present study we detected rapid growth in lesions 1 to 2 orders of magnitude larger, but only when DCA was present. This may reflect properties of cells in the lesions being selectively stimulated to grow by DCA. The phenotype of DCA-induced tumors is consistent with respect to c-Jun expression and lack of glycogen, although they are more heterogenous with respect to their staining with hematoxylin and eosin (Stauber and Bull, 1997). DCA also has substantial effects on the intermediary metabolism of the surrounding liver, acting to spare glucose by activating the pyruvate dehydrogenase kinase that normally inhibits TCA-cycle oxidations. The blood concentrations achieved by 2 g DCA/l of drinking water do exceed the apparent K_j of DCA for this enzyme (Kato-Weinstein et al., 1998). DCA-induced tumors have not been examined for their capacity for glycolytic metabolism, but higher rates of glycolysis are typical of some liver tumors. Therefore, the metabolic effects of DCA might also favor the growth of tumor cells that are not as dependent upon oxygen.

A model that accounts for saturation of DCA-promoted lesion growth by restoration of apoptosis might also explain why DCA sometimes appears to have initiating activity. Many initiated cells may undergo apoptosis before they are able to develop into preneoplastic foci; consequently, non-DNA reactive chemicals that promote tumor development by suppression of apoptosis may appear to have genotoxic activity because they

increase the efficiency of spontaneous initiation (Schulte-Hermann et al., 1993). Snyder et al. (1995) found that apoptosis in normal liver was substantially suppressed by even low doses of DCA. Thus, increased numbers of lesions could result from DCAs ability to inhibit apoptosis coupled to the demonstrated ability of DCA to increase replication rates within tumors at high doses (Stauber and Bull, 1997). We used parameters derived from our analysis of growth-rate data by Tan's model to determine the implications of this mechanism for the size distribution of non-extinct DCA-responsive clones after treatment for 52 weeks. This model predicts results that are qualitatively similar to data obtained by Stauber and Bull (1997).

The predominance of small lesions in DCA-treated animals may also account for the *LacI* mutations observed with chronic treatment for 60 weeks at 3.5 g/l (Leavitt et al., 1997). While these investigators were careful to insure that their tissue samples did not include tumor tissue, numerous small clones of cells with higher than normal replication rates could not have been reasonably excluded by their experimental technique. The hypothesis that such clones are present in the liver of DCA-treated mice is supported by direct observation (Stauber and Bull, 1997) and by the theoretical work presented here, which is consistent with growth rates observed for macroscopic lesions. Therefore, it is probable that the increased numbers of mutants recovered by Leavitt et al. (1997) is due to clonal expansion within the microscopic lesions observed by Stauber and Bull (1997). These data could also account for the apparent 'initiating activity' suggested by the fact that relatively short treatments (10–20 weeks) to high doses of DCA gave rise to tumors over the lifetime of animals.

We believe that these limited data are sufficient to illustrate the value of tumor imaging methods in collecting critical information on a carcinogen's mode of action. At the same time, it is important to recognize that these data address phenomena that occur at concentrations of DCA ≥ 2 g/l of drinking water. Treatment with 0.5 g/l produces a liver tumor incidence $> 80\%$ if mice are given sufficient time for tumor development at the

slower growth rates (DeAngelo et al., 1996; Stauber et al., 1998). Stauber et al. (1998) found that hepatocyte suspensions derived from B6C3F1 mice could be induced to form colonies on soft agar by concentrations of DCA more than an order of magnitude smaller than peak concentrations in the blood of mice treated with 2 g/l of DCA. The c-Jun + phenotype of these cells was identical to that observed in tumors induced by DCA, but not tumors or colonies induced by TCA. Therefore, it appears that growth of spontaneously initiated cell populations may be the source of tumors produced by DCA, even at low concentrations. In combination with the data of Snyder et al. (1995), the present data suggest that DCA could contribute to the efficiency of these 'initiating events' by simply suppressing apoptosis in these cell populations.

In summary, through the use of MR imaging it was shown that high doses of DCA have large effects on the growth rates of liver tumors. The data provided in this study, coupled with previous observations in our laboratory and others, strongly suggest that the primary effect of DCA in tumor induction is mediated through accelerated growth of spontaneously initiated cells.

At low doses DCA appears to suppress apoptosis (Snyder et al., 1995). Substantial increase in tumor cell replication superimposed on inhibition of apoptosis provides a reasonable basis for explaining the lesion size distribution observed in previous studies (Stauber and Bull, 1997). These results do not rule out a genotoxic effect by DCA, but simply indicate that direct interaction with DNA may not be necessary to explain its carcinogenic activity.

References

- Abramowitz, M., Stegun, I.A., 1965. Handbook of Mathematical Functions. Dover, New York, pp. 227–252.
- Bull, R.J., Sanchez, I.M., Nelson, M.A., Larson, J.L., Lansing, A.J., 1990. Liver tumor induction in B6C3F1 mice by dichloroacetate and trichloroacetate. *Toxicology* 63, 341–359.
- Chen, C., Farland, W., 1991. Incorporating cell proliferation in quantitative cancer risk assessment: Approaches, issues and uncertainties. In: Chemically Induced Cell Proliferation: Implications for Risk Assessment. Wiley-Liss, pp. 481–499.
- Daniel, F.B., DeAngelo, A.B., Stober, J.A., Olson, G.R., Page, N.P., 1992. Hepatocarcinogenicity of chloral hydrate, 2-chloroacetaldehyde, and dichloroacetic acid in male B6C3F1 mouse. *Fundam. Appl. Toxicol.* 19, 159–168.
- DeAngelo, A.B., Daniel, F.B., Stober, J.A., Olson, G.R., 1991. The carcinogenicity of dichloroacetic acid in the male B6C3F1 mouse. *Fundam. Appl. Toxicol.* 16, 337–347.
- DeAngelo, A.B., Daniel, F.B., Most, B.M., Olson, G.R., 1996. The carcinogenicity of dichloroacetic acid in the male Fischer 344 rat. *Toxicology* 114, 207–221.
- Dewanji, A., Venzon, D.J., Moolgavkar, S.H., 1989. A stochastic two-stage model for cancer risk assessment. II.: the number and size of premalignant clones. *Risk Anal.* 9, 179–187.
- Edelman, R.R., Hesselink, J.R., Zlatkin, M.B. (editors), (1996) *Clinical Magnetic Resonance Imaging*, second edition, W.B. Sanders Company.
- Farber, E., Sarma, D.S.R., 1987. Biology and disease, hepatocarcinogenesis: a dynamic cellular prospective. *Lab. Invest.* 56, 4–20.
- Folkman, J., Hockberg, M., Kinghton, D., 1974. In: Clarkson, B., Baserga, R. (Eds.), *Control of Proliferation in Animal Cells*. Cold Spring Harbor Laboratory Press, Cold Spring Harbor.
- Fox, A.W., Yang, X., Murli, H., Lawlor, T.E., Cifone, M.A., Reno, F.E., 1996. Absence of mutagenic effects of sodium dichloroacetate. *Fundam. Appl. Toxicol.* 32, 87–95.
- Giller, S., LeCurieux, F., Erb, F., Marzin, D., 1997. Comparative genotoxicity of halogenated acetic acids found in drinking water. *Mutagenesis* 12, 321–328.
- Grasl-Kraupp, B., Ruttkey-Nedecky, R., Mullauer, L., Taper, H., Huber, W., Bursch, W. and Schulte-Hermann, R., 1997. Inherent increase of apoptosis in liver tumors: Implications for carcinogenesis and tumor progression. *Hepatology* 25, 906–912.
- Leavitt, S.A., DeAngelo, A.B., George, M.H., Ross, J.A., 1997. Assessment of the mutagenicity of dichloroacetic acid in lacI transgenic B6C3F1 mouse liver. *Carcinogenesis* 18, 2101–2106.
- Harrington-Brock, K., Doerr, C.L., Moore, M.M., 1998. Mutagenicity of three disinfection by-products: di- and trichloroacetic acid and chloral hydrate in L5178Y/TK + /-3,7,2C mouse lymphoma cells. *Mutat. Res.* 413, 265–276.
- Herren-Freund, S.L., Pereira, M.A., Khoury, M.D., Olson, G., 1987. The carcinogenicity of trichloroethylene and its metabolites, trichloroacetic acid and dichloroacetic acid in mouse liver. *Toxicol. Appl. Pharmacol.* 90, 183–189.
- Kato-Weinstein, J., Lingohr, M.K., Thrall, B.D., Bull, R.J., 1998. Effects of dichloroacetate treatment on carbohydrate metabolism in B6C3F1 mice. *Toxicology* 130, 141–154.
- Kendall, D., 1948. On the generalized birth-death process. *AMS* 19, 1–15.

- Krasner, S.W., McGuire, M.J., Jacangelo, J.G., Patania, N.L., Reagan, K.M., Aetia, E.M., 1989. Occurrence of disinfection by-products in U.S. drinking water. *J. Am. Water Works Assoc.* 81, 41–53.
- Luebeck, E.G., Moolgavkar, S.H., 1991. Stochastic analysis of intermediate lesions in carcinogenesis experiments. *Risk Anal.* 11, 149–157.
- Minard, K.M., Wind, R.A., Bull, R.J., Miller, J.H., 1997. In vivo magnetic resonance imaging of DCA-induced hepatic lesions in male B6C3F1 mice. In: *Book of Abstracts: 5th Annual Meeting of The International Society for Magnetic Resonance in Medicine*, Berkeley, California: Society of Magnetic Resonance, p. 938.
- Minard, K.M., Wind, R.A., Phelps, R.L., 1998. A compact respiratory-triggering device for routine microimaging of laboratory mice. *JMRI* 8, 1343–1348.
- Moolgavkar, S.H., 1989. Multistage models for cancer risk assessment. In: Travis, C.C. (Ed.), *Biologically Based Methods for Cancer Risk Assessment*, NATO ASI Series A: Life Sciences, vol. 159. Plenum, New York, pp. 9–20.
- Moolgavkar, S.H., Luebeck, E.G., de Gunst, M., Port, R.E., Scharz, M., 1990. Quantitative analysis of enzyme-altered foci in rat hepatocarcinogenesis experiments I: single agent regimen. *Carcinogenesis* 11, 1271–1278.
- Pereira, M.A., 1996. Carcinogenic activity of dichloroacetic acid and trichloroacetic acid in the liver of female B6C3F1 mice. *Fundam. Appl. Toxicol.* 31, 192–199.
- Pereira, M.A., Phelps, J.B., 1996. Promotion by dichloroacetic acid and trichloroacetic acid of N-methyl-N-nitrosourea-initiated cancer in the liver of B6C3F1 mice. *Cancer Lett.* 102, 133–141.
- Schulte-Hermann, R., Bursch, W., Kraupp-Grasl, B., Oberhammer, F., Wagner, A., Jirtle, R., 1993. Cell proliferation and apoptosis in normal liver and preneoplastic foci. *Environ. Health Perspect.* 101, 87–90.
- Stauber, A.J., Bull, R.J., 1997. Differences in phenotype and cell replicative behavior of hepatic tumors induced by dichloroacetate (DCA) and trichloroacetate (TCA). *Toxicol. Appl. Pharmacol.* 144, 235–246.
- Stauber, A.J., Bull, R.J., Thrall, B.D., 1998. Dichloroacetate and trichloroacetate promote clonal expansion of anchorage-independent hepatocytes in vivo and in vitro. *Toxicol. Appl. Pharmacol.* 150, 287–294.
- Snyder, R.D., Pullman, J., Carter, J.H., Carter, H.W., DeAngelo, A.B., 1995. In vivo administration of dichloroacetic acid suppresses spontaneous apoptosis in murine hepatocytes. *Cancer Res.* 55, 3702–3705.
- Tan, W.Y., 1986. A stochastic Gompertz birth-death process. *Stat. Prob. Lett.* 4, 25–28.